Surface Plasmon Raman Scattering Studies of Liquid Crystal Anchoring on Liquid-Crystal-Based Self-Assembled Monolayers

ARTICLE *in* THE JOURNAL OF PHYSICAL CHEMISTRY B · NOVEMBER 2009

Impact Factor: 3.3 · DOI: 10.1021/jp907497p · Source: PubMed

Surface Plasmon Raman Scattering Studies of Liquid Crystal Anchoring on Liquid-Crystal-Based Self-Assembled Monolayers

Kevin Critchley,[†] Edward M. Cheadle,[†] Hao-Li Zhang,[†] Kurt J. Baldwin,[†] Quanying Liu,[‡] Yaling Cheng,[‡] Hitoshi Fukushima,[‡] Takashi Tamaki,[⊥] David N. Batchelder,[†] Richard J. Bushby,[‡] and Stephen D. Evans*,[†]

School of Physics and Astronomy, University of Leeds, Leeds, LS2, 9JT, United Kingdom

Received: August 04, 2009; Revised Manuscript Received: September 29, 2009

We studied the anchoring of 6CB on a series of self-assembled monolayers (SAMs) with a functional group that mimics that of the nematic liquid crystal (LC). The SAMs were first characterized by wetting, Fourier-transform infrared spectroscopy, and surface potential measurements. We found that, in two of these SAMs, the end group dipoles were oriented close to the normal of the surface and that these promoted homeotropic anchoring. In the case of the other SAM, the dipole was oriented parallel to the surface, and planar anchoring was obtained. Raman scattering by adsorbates on thin metal films is enhanced by the electromagnetic fields of surface plasmon polaritons (SPPs). Despite the inherent polarization of SPPs, there have been few reports in which SPP Raman scattering has been used to study molecular orientation. We have developed optical instrumentation to provide efficient excitation and collection of SPP Raman scattered light using attenuated total reflection geometry. The Kretschmann prism coupling configuration was used to excite SPPs on thin (500 Å) gold films with adsorbed SAMs of alkanethiols in contact with thin films (50 μm) of the nematic liquid crystal 4′-hexylbiphenyl-4-carbonitrile (6CB, Merck). The anchoring and orientational wetting of the LC 6CB at the interface with ω-functionalized SAMs was studied using this arrangement. In agreement with the results of previous studies, a high-energy surface ($-$COOH) was found to promote planar anchoring, whereas a low-energy surface ($-CF_3$) was found to induce homeotropic anchoring.

Introduction

Self-assembled monolayers (SAMs) have been used to promote alignment of nematic liquid crystals (LCs).[1−27] Many of these studies have concentrated on the use of SAMs to generate "high"- and "low"-energy surfaces to achieve alignment.[1−27] Few studies have dealt with the case when the functional group of the SAM is an LC look-alike. In this situation, the strong interactions between the functional group and LC allow one to control the alignment of the LC simply by selecting the orientation of the functional group of the SAM. Therefore, in this study, we use novel SAM materials that have functional groups that mimic nematic LCs (Figure 1a). The question is, can changing the geometry of the LC mimicking group of the SAM, with respect to the surface, promote "homeotropic" or "planar" alignment of a LC film (Figure 1b)? It is known that the orientation of the first molecular layer of the LC, which is in contact with the substrate, influences the director orientation for the order of tens of micrometers into the bulk of the LC. The relationship between the microscopic interactions, which influence the orientation of the first layer, and the mesoscopic alignment is not yet fully understood.[28,29] However, a full understanding of this relationship is required if surfaces are to be engineered to control LC anchoring. Such control is of importance technologically where the anchoring of low-molecular-weight nematics is crucial to the function of LC displays. Liquid crystal surface interactions have also been exploited for chemical and biological sensing and for the generation of templates for the production of inorganic materials.[3,7,17,30−34]

The use of SAMs of alkanethiols for the study of LC/surface interactions has been pioneered by Abbott[1−18] and Evans.[19−27] The work of Abbott has concentrated mainly on polarized light microscopy and interferometer studies of the alignment of 4′-pentylbiphenyl-4-carbonitrile (5CB) in SAM-functionalized planar cells (2−30 μm thick). In cells functionalized with single-component SAMs of alkanethiols, Drawhorn and Abbott found planar anchoring.[6] This was in contrast to the results obtained for low-energy surfaces formed by aliphatic monolayers on silica and germanium that promoted homeotropic anchoring.[13] It has been postulated that the planar anchoring of 5CB on $-CH_3$-functionalized SAMs (on gold) is due to the anisotropic dispersion interactions between the LC and the gold substrate.

Evans has concentrated on the study of the LC/SAM interface using an ensemble of evanescent wave techniques: evanescent Brewster angle ellipsometry,[20−22] surface plasmon resonance (SPR) imaging,[23] and attenuated total reflection infrared (ATR-IR) spectroscopy.[24] Using evanescent Brewster angle ellipsometry with SAM-modified gold substrates, Evans and co-workers were able to obtain a phase diagram showing both the presence of an anchoring transition and orientational wetting.[20−22] In all cases of homeotropic anchoring, complete orientational wetting was seen as $T \rightarrow T_{IN}$. Planar anchoring, on the other hand, was always associated with nonwetting or partial wetting of the isotropic/SAM interface. These results suggested that the driving

* Corresponding author. Phone: +441133433852. E-mail: s.d.evans@leeds.ac.uk.

[†] School of Physics and Astronomy, University of Leeds.

[‡] Current address: Centre for Self Organising Molecular Systems, University of Leeds.

[‡] Current address: New Domain Research & Development Centre, Tsukuba Branch of Bioresearch Laboratory, Seiko Epson Corporation, Okubo 2, Tsukuba-city, Ibaraki-ken 300-2611, Japan.

[⊥] Current address: Institute for Materials and Chemical Process (IMCP), National Institute of Advanced Industrial Science and Technology (AIST), Tsukuba, Ibaraki 305-8562, Japan.

10.1021/jp907497p CCC: $40.75
Published on Web 10/29/2009

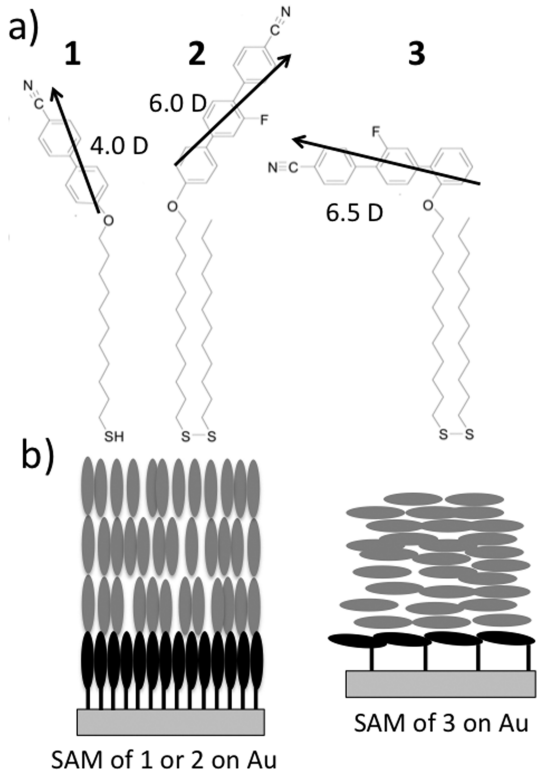

Figure 1. Molecular formulas of the SAM-forming materials (**1**, **2**, and **3**) used in this study (a). Molecular modeling of the rigid biphenyl/terphenyl moiety using a semiempirical method showed that the net dipole moment lies approximately along the long axis in each case; however, it must be noted that this does not account for any dipoles associated with the alkyl chains and that the time-averaged orientation of the dipole moments would be affected by rotation about the single bonds. (b) A cartoon of homeotropic nematic liquid crystal (4′-hexylbiphenyl-4-carbonitrile, 6CB) alignment on SAMs of **1** and **2** (left) and planar anchoring of 6CB on SAMs of **3** (right).

forces responsible for orientational wetting and anchoring were closely related.[21] It is thought that for the case of a low-energy surface, *n*CB−*n*CB interactions (dipole−dipole interactions which favor dimer formation) dominate, resulting in homeotropic anchoring and complete wetting of nematic at the isotropic/substrate interface. However, high-energy surfaces favor wall−liquid interactions, leading to planar anchoring and a disruption of "dimer" correlations, preventing orientational wetting of the interface.

Evanescent Brewster angle ellipsometry studies measure an integrated orientational adsorption for the interfacial region lying within the range of the evanescent field generated at the LC/SAM interface. Although these measurements can distinguish between planar and homeotropic anchoring, they cannot quantitatively separate changes in orientation from variations in film thickness or anchoring strength. An "ideal" measurement would separate out changes in orientation from changes in thickness for nematic films adsorbed at the LC/substrate interface.[28] Doing so for a nematic film adsorbed at the substrate/isotropic interface would yield a microscopic orientational order parameter.

The motivation behind the development of the instrument described in this work was to use evanescent wave Raman scattering to measure microscopic orientational order parameters for the interface between SAMs of alkanethiols on gold and LCs. Making such a measurement would test the hypothesis of Evans and co-workers discussed previously that the case of complete pretransitional orientational wetting observed for low energy surfaces is due to the dominance of *n*CB-*n*CB interactions over liquid−wall interactions.[20,35,36] Since functionalization of any total internal reflection element with SAMs of alkanethiols requires the use of an intermediate layer, it was decided that the evanescent fields of surface plasmon polaritons (SPPs) excited at the gold/SAM interface should be utilized to probe the LC/SAM interface.

Raman scattering by adsorbates on thin metal films is known to be enhanced by the electromagnetic fields of SPPs.[37−48] Previous studies have investigated this effect using liquids[38,39] and utilized the enhancement to record Raman spectra of ultrathin organic films.[39−47] Despite the inherent polarization of SPPs, there have been few reports in which SPP Raman scattering has been used to study molecular orientation.[41] However, it was suggested by Corn and Philpott that SPP Raman scattering could analyze the LC/solid interface. No study of this kind has been published.[39] Here, SPP Raman scattering experiments were performed to study the degree of orientational order at the LC/SAM interface as a function of temperature, T, in the region of the isotropic to nematic phase transition T_{IN}. We first study the interaction of the LC 4′-hexylbiphenyl-4-carbonitrile (6CB) with low- and high-energy surfaces using alkanethiol SAMs of $HS(CH_2)_{11}(CF_2)_9CF_3$ and $HS(CH_2)_{10}CO_2H$.[21,22] Since this is the first time surface plasmon Raman scattering has been used to study the anchoring of LCs on SAMs, we first study the interaction of alkanethiol SAMs of $HS(CH_2)_{11}(CF_2)_9CF_3$ and $HS(CH_2)_{10}CO_2H$ and make comparison with other techniques from previous studies.[21,22] These surfaces act as references to compare the results collected using the surface plasmon Raman scattering technique and the results obtained from previous methods.[21,22] The low- and high-energy surfaces are well-characterized and typically form highly ordered films.

In this paper, we focus on novel SAMs with functional groups that "mimic" the LC to control LC anchoring of 6CB.[19,49−55] The first part of the results section deals with the characterization of SAMs formed from the 4′-bound biphenyl **1** and the 4″-bound terphenyl **2**, where the molecular dipole is close to perpendicular to the surface (Figure 1a). By changing the covalent anchoring point of the terphenyl to 2″, as in **3**, it is possible to create a SAM in which the molecular dipole lies almost parallel to the surface.[50] The difference between the functional groups of SAMs of **1** (or **2**) and **3** has a direct influence on the LC anchoring (Figure 1b). In this work, we study the LC alignment on each of these SAMs using the surface plasmon Raman scattering system described.

Experimental Section

Materials. The synthesis of **2** is reported elsewhere.[49] The syntheses scheme of **1** and **3** are summarized in the Supporting Information. The nematic liquid crystal used throughout this study was 4′-hexylbiphenyl-4-carbonitrile (6CB, Merck). All other materials were acquired commercially without further modification. Molecular modeling of **1**, **2**, and **3** was achieved using the HyperChem software package using a semiempirical method (AM1).

Contact Angle Measurements. The samples were placed on a stage beneath a square-cut needle with a 0.5 mm bore. Sessile drops of water, ethylene glycol, and methylene iodide were formed using a glass capillary tube. The drops were illuminated from behind by a sodium lamp and imaged using a Navitar zoom lens coupled to a ×2 extension tube (total magnification of up to ×22) on a Hamamatsu C3077 CCD camera. The images were viewed on a high-resolution monochrome video monitor and captured and measured using Accuware software. Measurements

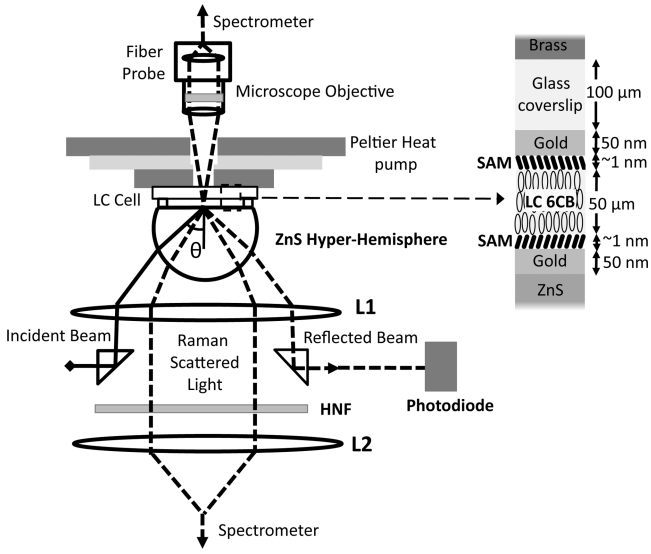

Figure 2. Schematic illustration showing the experimental setup for SPP Raman scattering studies of the LC/SAM interface. Solid lines represent the incident light; dashed lines represent the reflected and scattered light. Raman scattered light was collected through L1 for all experiments unless stated otherwise. A schematic (not to scale) of the LC cell is shown to the right.

were made at room temperature (~23 °C). Contact angles quoted in this report were an average of at least six measurements.

Surface Potential Measurements. A traditional Kelvin probe was used to measure the surface potential of the thin films in air. The Kelvin probe technique is described elsewhere.[56−59] The reference electrode was a platinum tip of area 2.7 mm^2, which was oscillated with a piezo actuator at 800 Hz. The sample was manipulated on an x, y, and z stage until the tip−sample separation was approximately 20 μm. At this distance, the change in capacitance, due to the oscillation, between tip and sample causes an alternating current to flow. The alternating current was measured using a Perkin-Elmer model 7220 DSP Lock-in amplifier. A bias placed across the tip and sample was adjusted until the lock-in signal was nullified. At this value, the applied bias will be equal and of the opposite sign to the contact potential difference (CPD). The surface potential can be calculated by measuring the difference between the CPD of the substrate before and after absorption of a SAM. Measurements were made at room temperature (~23 °C). At least six measurements were made on each sample.

Reflection Absorption Infrared Spectroscopy (RAIRS). RAIRS spectra of the SAMs were collected at an incident angle of 80° using a Bruker IFS-48 spectrometer equipped with a high-sensitivity DTGS detector. Spectra were taken after purging in dry air for at least 16 h. A reference spectrum of gold freshly cleaned under the same conditions was subtracted. Spectra were collected for 2000 scans at a resolution of 2 cm^{-1}.

Surface Plasmon Polariton Raman Scattering Measurements. A schematic illustration of the symmetric 50 μm LC cell and integrated excitation/collection optics used in the experiments described here is shown in Figure 2. Using the Kretschmann prism-coupling configuration, SPPs were excited on evaporated thin (500 Å) gold films with adsorbed SAMs of alkanethiols. Following the experimental configuration of Futamata,[45−47] a truncated hemispherical prism, known as a Weierstrass prism, was combined with a high numerical aperture (NA) condensing objective (Aspherab, Oriel) to enable efficient collection of the out-coupled Raman scattered light.[45−47] By using a Weierstrass prism and high NA objective, collection of the whole cone of out-coupled SPP Raman scattered light (with a half angle α) was possible. The Weierstrass prism used here was manufactured by Crystran Ltd. (Poole, England) from zinc sulfide (ZnS CLEARTRAN, Rohm and Haas Advanced Materials). ZnS CLEARTRAN has a low spectral background between 1000 and 3000 cm$^{-1,}$ and its refractive index (n_{ZnS} (633 nm) = 2.35), is sufficient for the excitation of SPPs on a thin gold film in contact with homeotropically aligned 6CB (n_{6CB} (633 nm) = 1.69) when incident using radiation at 633 nm. The angle of incidence, θ, of the exciting laser beam (He−Ne, 633 nm ~3mW) was controlled by means of a beam-steering prism mounted on a computer-driven translation stage in the back plane of the condensing objective. A holographic notch filter placed in the collimated beam behind the condensing objective removed the out-coupled Rayleigh scattered light, and an achromatic doublet focused the remaining collimated Raman scattered light onto a fiber optic bundle. Unless stated otherwise, the Raman scattered light for the LC studies was collected through lens L1. Further discussion of this of the collection optics is presented in the Supporting Information. Raman intensity data are all normalized to their maximum value in the isotropic phase ($T - T_{IN} = 6.75$ K).

The fibers of this collection bundle were arranged as a slit at the entrance to a Reni Shaw System 100 Raman spectrometer. Code to integrate beneath a given range in the acquired Raman spectra was included in the software controlling θ; thus, SPR Raman intensity curves could be generated and recorded. Further details of the optical instrumentation can be found in ref 60. Symmetric planar liquid crystal cells were formed between the SAM-functionalized gold coating the flat face of the Zen's hyperhemisphere and an identically coated quartz coverslip (0.1−0.15 mm thick, Agar Scientific), as shown schematically in Figure 2. The cells were assembled by placing a small droplet of liquid crystal between two 50 μm polytetrafluoroethylene spacer strips (Goodfellow) on a coated coverslip. The temperature of the cell was controlled to a precision of ±0.01 K over the temperature range 293−313 K. An annular heater/cooler assembly was used, utilizing a Peltier device with a 3-mm-diameter center hole as shown in Figure 2. This allowed optical access to the front of the cell so that Raman scattered light could be collected using a microscope objective and Renishaw compact fiber optic probe. The hole through the center of the heater/cooler device was just large enough to exploit the full NA (0.35) of the Olympus SLMPLAN × 20 microscope objective. Thus, a comparison could be made between Raman spectra acquired using light scattered to the LC and gathered though the LC cell to the out-coupled Raman scattered light collected using the Weierstrass prism and condensing objective. The ZnS prisms were recleaned approximately six times before being replaced due to deterioration in the signal.

Results and Discussion

The SAMs were characterized using a combination of surface science techniques, including FTIR spectroscopy, contact angle goniometry, and surface potential measurements. The average molecular orientation within the SAMs of **2** and **3** have previously been determined using a combination of RAIRS and SFG.[50] It was found that for SAMs of **2**, the chromophore was oriented nearly normal to the plane of the surface (±28°), whereas for compound **3**, the chromophore was aligned in the plane of the surface (>80°). The CN stretching mode for SAMs of compounds **1**, **2**, and **3** are shown in Figure 3. From the spectra shown and consideration of the surface selection rule, it is evident that compound **1** is similar to **2**, that is, with the

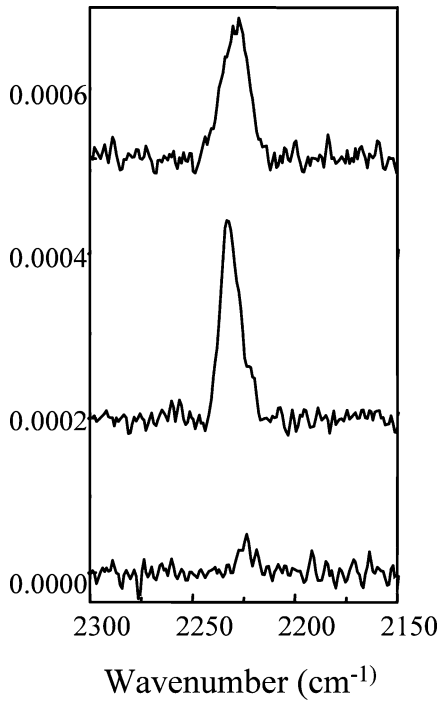

Figure 3. RAIRS spectra showing the CN stretching mode from SAMs formed by compounds **1**−**3** on a gold substrate.

TABLE 1: Summary of Contact Angle and Surface Potential Results for SAMS of 1, 2, and 3

SAM	contact angle/°			surface potential/mV
	water	methylene iodide	ethylene glycol	
1	60	44	24	−306
2	61	48	28	−377
3	84	60	36	154

CN mode nearly normal to the surface.[50,61] This conclusion is also supported by the spectra in the "mid" frequency region (Supporting Information). From a combination of the SAM reflectance spectrum and the KBr transmission spectrum, the average orientation of the rigid chromophore is estimated to be nearly normal (±30°) to the surface. The high frequency spectra are show in the Supporting Information. The contact angles of sessile droplets on each of the SAMs are presented in Table 1. The SAMs formed from compounds **1** and **2** showed an increased wettability by water as compared with that from compound **3**, and identical trends were seen for the polar liquids methylene iodide and ethylene glycol. This indicates an increased interaction between the polar liquids and SAMs when the surface dipoles are oriented normal to the surface as compared to SAMs with surface dipoles oriented in the plane of the surface.

The adsorption of a SAM onto a substrate has the effect of either increasing or decreasing the work function.[62,63] A positive surface potential (ΔV) implies a decrease in work function, whereas a negative value implies an increase in work function. The surface potential values of the SAMs formed from **1**−**3** are presented in Table 1. SAMs of **1** and **2** have negative surface potential values of a similar magnitude. The SAM of **3**, however, produced a positive surface potential, which implies a decrease in work function. The Demchak and Fort[64] model is used to interpret surface potential by considering the dipole contribution of the headgroup, μ_1/ε_1, and the tail group, μ_2/ε_2, of the adsorbent, as shown in eq 1,

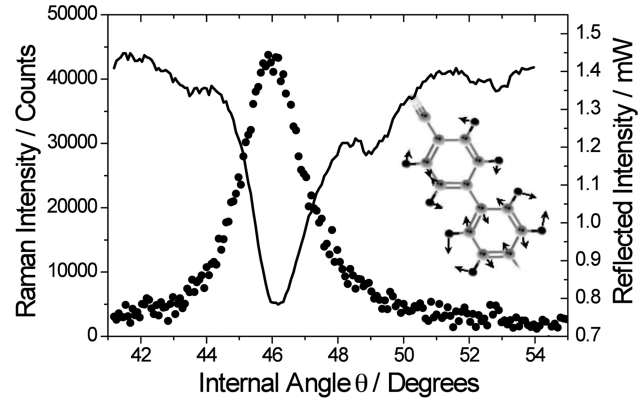

Figure 4. The integrated Raman intensity and reflected intensity as a function of internal angle θ, showing the enhancement in Raman intensity at the SPP resonance. The intensity of the Raman band at 1608 cm^{-1} was used, on the basis of a molecular model for this mode of vibration (insert).

$$\Delta V = \frac{n}{\varepsilon_0}\left[\frac{\mu_1}{\varepsilon_1} + \frac{\mu_2}{\varepsilon_2}\right] \quad (1)$$

where n is the packing density and ε_0 is the permittivity of free space.[65] Evans et al. estimated the headgroup contribution of alkanethiols SAMs (on gold) to be ∼0.24 D.[62] By making the assumption that the headgroup contribution should be the same for all alkanethiol SAMs, an estimate for the net "normal component" of the dipole moment can be made for SAMs of **1** and **2**. We estimate the dielectric constant of **1** and **2** along the axis to be 12.5 and 15.0, respectively, on the basis of the quoted dielectric constant along the axis of LC molecules of similar biphenyl and terphenyl structures.[66,67] The molecular packing density of SAMs of **1** and **2** are estimated to be 4.6×10^{18} molecules/m^2. Thus, the net normal component of the tail group dipole of **1** and **2** is calculated to be $\mu_2 = 5.2$ D and $\mu_2 = 6.9$ D, respectively. From molecular modeling (Figure 1), we expect the dipole moment of **1** (∼4.0 D) to be smaller than **2** (∼6.0 D), which is in good agreement with that calculated. It should be noted, however, that the packing densities of **1** and **2** might differ due the structural differences, including that **2** will have a contribution from the pure alkanethiolate chains (Figure 1a). The positive surface potential of the SAM of **3** suggests that the −C≡N dipole only has a small contribution to the surface potential; that is, the data constant with the molecular orientation found from the RAIRS data. The dielectric constant perpendicular to the axis of **3** is estimated to be 5.6 on the basis of data for LC molecules of a similar structure.[67] Applying a packing density of 2.5×10^{18} molecules/m^2 (on the basis of data obtain in reference[50]) would give the normal component of the net dipole moment of **3** to be ∼1.5 D; that is, much lower than both **1** and **2** and consistent with the net dipole moment orientation being close to parallel to the plane of the surface. In the case of SAMs of **3**, it is likely that the $-CH_3$ dipole contributes to the surface potential and partly explains the positive surface potential observed.

SPP Raman Scattering Studies of the LC/SAM Interface in the Region of the Isotropic-to-Nematic Transition. Initially, SPR Raman and reflected intensity curves were recorded with the LC in the isotropic phase (306 K). At first, the intensity of the out-coupled SPP Raman scattered light was monitored as a function of the internal angle of incidence θ of the excitation light. Figure 4 shows the integrated intensity of the band at 1608 cm^{-1}, assigned to the stretching of the phenyl rings of the 6CB molecules recorded as a function of θ, for p-polarized incident

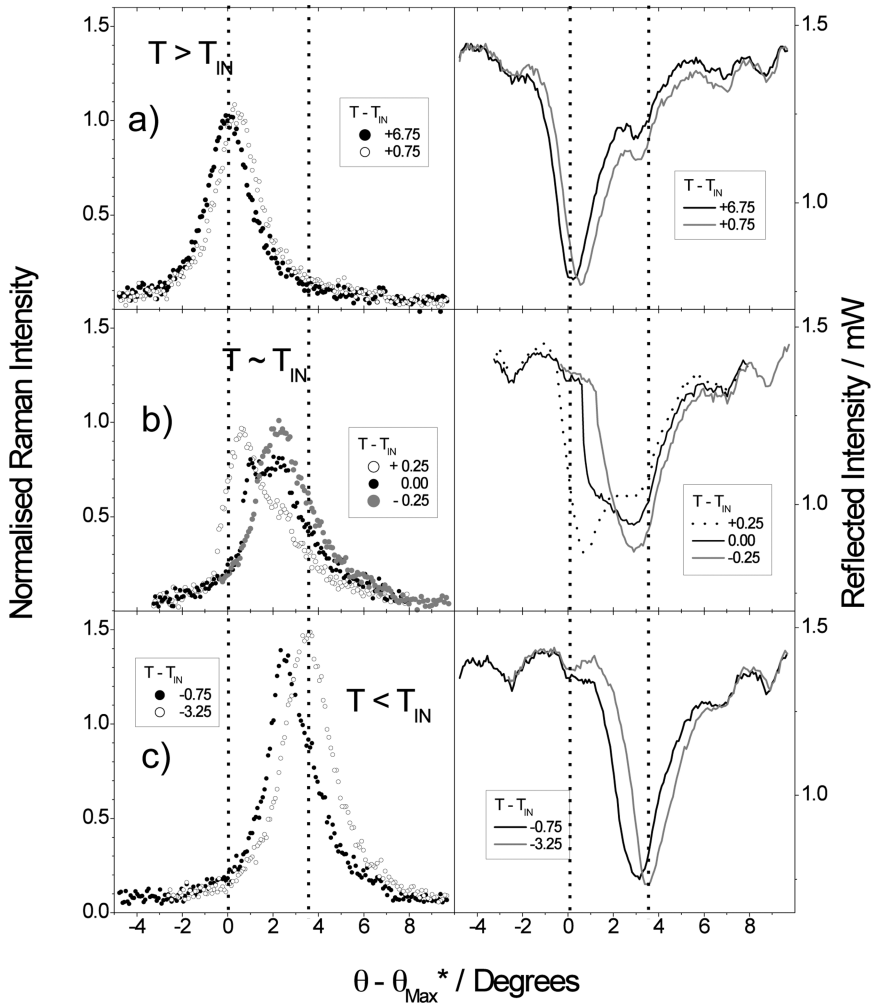

Figure 5. SPR Raman intensity and reflected intensity curves as a function of SPR angle upon cooling through the isotropic-to-nematic phase transition for the 6CB/CF_3 interface. The curves at temperatures above the nematic phase transition temperature T_{IN} (a), close to T_{IN} (b), and below T_{IN} (c) are presented. The Raman intensity was obtained by integrating beneath the band at 1608 cm^{-1}. Exposure times of 10 s were used to acquire the spectrum for each point on the SPR intensity curve. Angles are referenced to the angle of maximum intensity for the Raman intensity taken with the liquid crystal in the isotropic phase (A^*_{max}).

light.[68] The main symmetry axis of this vibration lies along the rigid LC core; hence, it has been used successfully in previous Raman scattering studies of nematic order.[35,36,69,70] The 1608 cm^{-1} Raman band was found to be the most intense of the bands of the LC core; therefore, using it minimized the time for the acquisition of each SPR curve.[71] The Raman scattered light was collected from behind the hyperhemisphere using L1 (Figure 2). A clear resonance in the Raman scattered intensity is seen, with a maximum intensity recorded at $\theta = \theta_{max} = 46.0°$. The concomitant resonant dip in the reflected intensity confirmed that the resonant enhancement of the Raman scattering was due to the excitation of SPPs at the metal/SAM interface. It is noted that the minimum in the reflectivity curve occurred at a slightly higher angle than the maximum on the Raman intensity curve. This apparent discrepancy can be partially explained when one considers that in the Kretchsmann geometry decay of the SPP mode at the gold/LC interface occurs via both Joule heating and out-coupling back into radiative bulk modes in the prism.[72,73] A comparison of collecting Raman scattered light from L1 and through the microscope objective is discussed in Supporting Information.

Studies of the Isotropic-to-Nematic Transition of High- and Low-Energy Surfaces. SAMs of semifluorinated ($HS(CH_2)_{11}(CF_2)_9CF_3$) and carboxylic acid ($HS(CH_2)_{11}COOH$)-terminated alkanethiol SAMs have been extensively studied elsewhere.[22,60,74−76] In this study, we have used the semifluorinated SAM and a carboxylic acid SAM to form low- and high-energy surfaces, respectively. The Peltier heat pump (Figure 2) first heated the LC cells above the isotropic−nematic phase transition T_{IN} (302 K) before being cooled through T_{IN} in a sequence of steps. At each temperature, the experiment was first left for several minutes to allow the cell and heater/cooler plate to equilibrate. After equilibration, SPR intensity curves were recorded for the Raman mode at 1608 cm^{-1}.

SPR Raman intensity curves for a cell functionalized with semifluorinated alkanethiol SAMs are shown in Figure 5. Upon cooling from the isotropic ($T - T_{IN} = +6.75$ K) to the nematic ($T - T_{IN} = -3.25$ K) phase, the SPR position was observed to shift to a higher angle of incidence. Concomitant with the positive shift in the SPR angle, an increase in the Raman intensity was recorded as the liquid crystal was cooled into the nematic phase. The positive shift in the SPR angle indicates an increase in the component of refractive index normal to the surface and, hence, homeotropic anchoring of the nematic director. These results are in agreement with those obtained for this system in Brewster angle ellipsometry experiments.[22] The increase seen in SPP Raman scattering intensity was expected for homeotropic anchoring, since the vibrations along the rigid

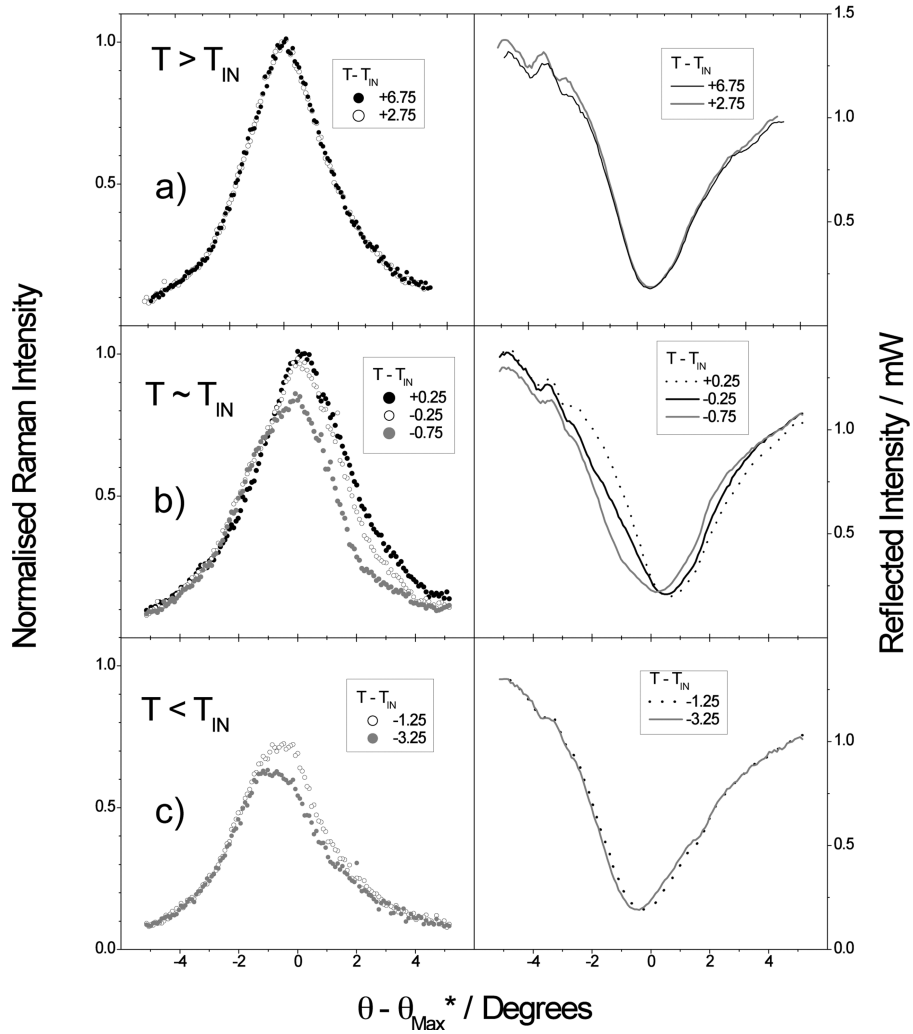

Figure 6. SPR Raman intensity and reflected intensity curves as a function of SPR angle upon cooling through the isotropic-to-nematic phase transition for the 6CB/COOH interface. The curves at temperatures above the nematic phase transition temperature T_{IN} (a), close to T_{IN} (b), and below T_{IN} (c) are presented. The Raman intensity was obtained by integrating beneath the band at 1608 cm^{-1}. Exposure times of 10 s were used to acquire the spectrum for each point on the SPR intensity curve. Angles are referenced to the angle of maximum intensity for the Raman intensity taken with the liquid crystal in the isotropic phase (A^*_{max}).

core of the molecules are preferentially aligned with the major component of the electric field due to the SPPs; that is, normal to the gold surface. This behavior has been treated as a class of wetting phenomena known as an approach to complete wetting.[23] Orientational wetting can be viewed as the adsorption of an A-rich film from a two-component (A−B) liquid mixture, where A is the nematic (oriented) phase. Reducing T toward T_{IN} is similar to varying the chemical potential of component A at fixed T, toward bulk two-phase coexistence of A-rich and B-rich fluids (i.e., nematic and isotropic), which in turn is equivalent to an adsorption isotherm experiment in the approach to saturation. Bulk two-phase coexistence of the nematic and isotropic phases was manifest in the appearance of a second component in the SPR curves recorded in the region $T \sim T_{IN}$ shown in Figure 5. Similar two-component SPR curves, resulting from two-phase coexistence at $T \sim T_{IN}$, were reported by Chu et al. in their SPR studies of the isotropic-to-nematic transition.[77] Later, using SPR imaging, Evans et al. imaged coexisting domains of isotropic and nematic LC at the LC/SAM interface at $T = T_{IN}$. For the SPR curves to have split in this way, the lateral size of the nematic/isotropic domains must have been less than the size of the incident beam at the prism/gold interface but larger than the propagation length, L_x, of the plasmons at the gold/SAM/LC interface.[77,78] From measurements of the spot size at the collection fiber, the incident beam diameter at the prism/gold interface was estimated to be ∼120 μm. L_x, was estimated from the calculations of Rothenhäusler and Knoll and Chu et al., to be on the order 4 μm.[77,78] The size of the nematic/isotropic domains probed in the experiments shown above was therefore estimated to be on the order 10−100 μm. It is noted that domains of this size can clearly be seen in the SPR micrographs of the LC/SAM interface taken by Evans et al. at $T = T_{IN}$.[23]

Figure 6 shows the SPR Raman intensity data for the case of the 6CB/COOH SAM interface. As the temperature of the LC cell is reduced below T_{IN}, the Raman intensity decreases. The decrease in Raman intensity for a mode along the biphenyl long axis indicates planar anchoring of the nematic phase. This conclusion is also confirmed by the negative shift in θ_{Max}, suggesting that the component of the refractive index of the LC normal to the surface decreases, as expected for planar anchoring. Alkahairalla et al. drew the same conclusions for the 6CB/COOH interface from Brewster angle ellipsometry experiments.[20,21] For the 6CB/COOH interface, no measurable variation in either Raman intensity or resonance angle was recorded above T_{IN}, indicating little or no temperature dependence on the interfacial structure. This implies partial wetting, or nonwetting, by nematic at the isotropic LC/SAM interface.[21,23]

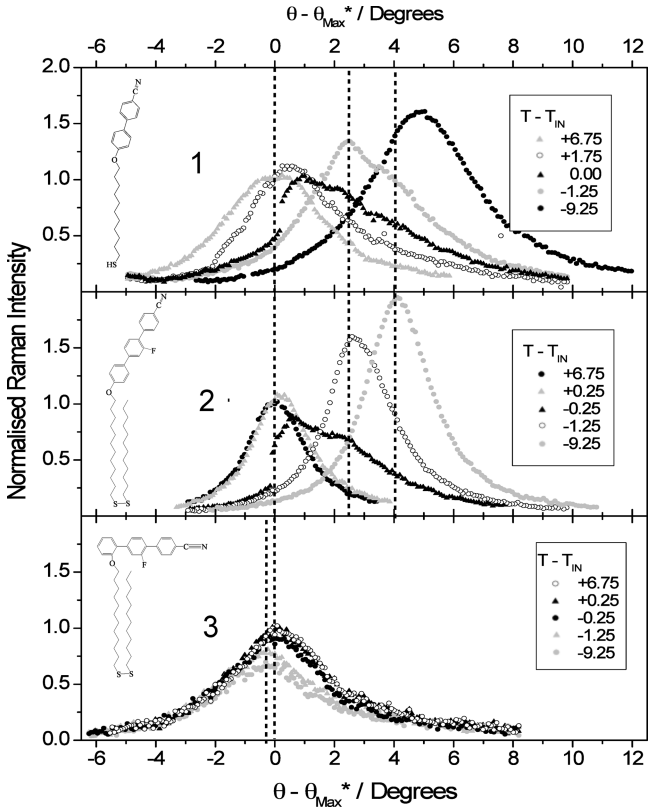

Figure 7. SPR Raman intensity curves upon cooling through the isotropic-to-nematic phase transition for the LC 6CB at the interface with SAMs formed from LC-like cyano-terminated alkanethiols **1**, **2**, and **3**. The Raman intensity was obtained by integrating beneath the band at 1608 cm^{-1}. Exposure times of 10 s were used to acquire the spectrum for each point on the SPR intensity curve. Angles are referenced to the angle of maximum (θ^*_{max}) intensity for the Raman intensity taken with the liquid crystal in the isotropic phase.

Interaction of 6CB with LC-Terminated SAMs 1, 2, and 3. LC cells, as described above, were functionalized with SAMs using compounds **1**−**3**. In Figure 7, SPR Raman intensity curves are shown for the LC mimicking SAM/6CB interfaces upon cooling from the isotropic to the nematic phase. For SAMs of **1** and **2**, which have a significant dipole orientated normal to the gold surface, an increase in Raman intensity and positive shift of θ_{max} were observed upon cooling from the isotropic to the nematic phase, indicating homeotropic anchoring of the director. Coexistence of isotropic and homotropic phases is observed close to the transition temperature, and since we are sensitive to the LC molecules close to the SAM/LC interface, we can conclude that the orientation wetting grows from the LC SAM interface. This information gives a clearer picture than given by previous evanescent ellipsometric studies. The continuous nature of the growth of this phase as T approaches T_{IN} indicates that, as for homeotropic anchoring on low energy surfaces, complete orientational wetting occurs. SAMs of **3**, on the other hand, pinned the nematic director parallel to the surface (planar anchoring), leading to a decrease in both the SPP resonance angle and Raman intensity upon cooling from the isotropic to the nematic phase. A much smaller change in angle is observed due to the difference in refractive index between isotropic and planner anchoring being smaller than for isotropic-to-homeotropic alignment (as in the case of **1** and **2**). It is noted that the increased breadth of the SPR curves recorded in the isotropic phase for the **1** and **3** samples is thought to be due to an increase in the roughness of the ZnS/gold interface due to cleaning and reuse of the ZnS Weierstrass prisms. The disadvantage of current instrumentation is that orientation parameters cannot be calculated from the data, since this requires evanescent Raman scattering to access both s- and p-polarized light.

Conclusions

A series of SAMs, which gave arrays of oriented surface dipoles, were formed using an alkanethiol and two dialkyl disulfides, all three of which were terminated with LC-like moieties. SPP Raman scattering studies showed that the orientation of the LC portion of these molecules was by controlled anchoring of the nematic director of an overlayer of 6CB. SAMs of **1** and **2** had their rigid core oriented normal to the surface and induced homeotropic anchoring, whereas **3**, which has dipoles oriented in the plane of the surface, pinned the nematic director parallel to the surface. In agreement with previous studies, all SAM substrates that induced homeotropic anchoring also promoted complete wetting of the isotropic/SAM interface for $T \rightarrow T_{IN}$, whereas non- or partial wetting was seen in the same temperature range on substrates that caused planar alignment of nematic director. In terms of instrumentation, collection of the out-coupled SPP Raman scattered light was essential for obtaining accurate measurements of the Raman scattered intensity from the LC/SAM interface. The interfacial sensitivity of this evanescent wave technique has enabled the discrimination of pretransitional nematic thin films adsorbed at the isotropic LC/SAM interface. For 6CB supported by a SAM giving a low surface free energy (formed using a semifluorinated alkanethiol), homeotropic anchoring was observed upon entering the nematic phase, whereas a SAM giving a high surface free energy (formed using a carboxylic acid-terminated alkanethiol) was seen to promote planar anchoring. These results are in direct agreement with those of previous evanescent Brewster angle ellipsometry, SPR, and ATR-IR experiments conducted on similar LC/SAM interfaces.[21−23]

The presence of the gold layer (between the prism and SAM), required for SAM functionalization and utilized in the generation of SPPs, drastically reduced the Raman scattered intensity recorded using s-polarized incident light.[60] This prevented the measurement of the Raman depolarization ratios required for the determination of orientational order parameters for the LC/SAM interface.[35,36,60,70] It is noted that Noble-Luginbuhl and Nuzzo have demonstrated the formation of SAMs of alkanethiols directly on zinc selenide (ZnSe) substrates.[79]

Prism functionalization using this method would allow an increase in the intensity of the s-polarized evanescent field at the LC/SAM interface; however, since SPPs could no longer be generated, it would lead to a decrease in the maximum intensity of the evanescent field. It should also be noted that although the presence of the metal layer prevented the measurement of microscopic orientation order parameters, the SPPs generated at the metal/SAM/LC interface provided important information on the lateral structure of the interface in the region of coexistence ($T \sim T_{IN}$). It is noted that such information is not provided by evanescent wave ellipsometry techniques.

Acknowledgment. E.C. and K.C. acknowledge receipt of EPSRC CASE studentships with the Seiko Epson Corporation. E.C. acknowledge the advice of Dr. Masayuki Futamata on the construction and use of the SPP Raman instrumentation. For technical assistance with the instrument and control software at the University of Leeds, E.C. thanks Mr. Brian Gibb, Mr. Robert Henderson, and Dr. Grant Thompson. We dedicate this manuscript to David Batchelder for his devotion to, and expertise in, the development in Raman microscopy.

Supporting Information Available: The full details of the syntheses of **1** and **3**, including the spectroscopic and analytical data, mid- and high-frequency IR data, and further details of the optical instrumentation. This material is available free of charge via the Internet at http://pubs.acs.org

References and Notes

(1) Abbott, N. L. *Curr. Opin. Colloid Interface Sci.* **1997**, *2*, 76.
(2) Cadwell, K. D.; Alf, M. E.; Abbott, N. L. *J. Phys. Chem. B* **2006**, *110*, 26081.
(3) Cadwell, K. D.; Lockwood, N. A.; Nellis, B. A.; Alf, M. E.; Willis, C. R.; Abbott, N. L. *Sens. Actuators, B* **2007**, *128*, 91.
(4) Clare, B. H.; Efimenko, K.; Fischer, D. A.; Genzer, J.; Abbott, N. L. *Chem. Mater.* **2006**, *18*, 2357.
(5) Clare, B. H.; Guzman, O.; de Pablo, J. J.; Abbott, N. L. *Langmuir* **2006**, *22*, 4654.
(6) Drawhorn, R. A.; Abbott, N. L. *J. Phys. Chem.* **1995**, *99*, 16511.
(7) Govindaraju, T.; Bertics, P. J.; Raines, R. T.; Abbott, N. L. *J. Am. Chem. Soc.* **2007**, *129*, 11223.
(8) Gupta, V. K.; Abbott, N. L. *Langmuir* **1996**, *12*, 2587.
(9) Gupta, V. K.; Abbott, N. L. *Phys. Rev. E* **1996**, *54*, R4540.
(10) Gupta, V. K.; Abbott, N. L. *Science* **1997**, *276*, 1533.
(11) Luk, Y. Y.; Tingey, M. L.; Dickson, K. A.; Raines, R. T.; Abbott, N. L. *J. Am. Chem. Soc.* **2004**, *126*, 9024.
(12) Luk, Y. Y.; Yang, K. L.; Cadwell, K.; Abbott, N. L. *Surf. Sci.* **2004**, *570*, 43.
(13) Miller, W. J.; Abbott, N. L.; Paul, J. D.; Prentiss, M. G. *Appl. Phys. Lett.* **1996**, *69*, 1852.
(14) Miller, W. J.; Gupta, V. K.; Abbott, N. L.; Tsao, M. W.; Rabolt, J. F. *Liq. Cryst.* **1997**, *23*, 175.
(15) Park, J. S.; Jang, C. H.; Tingey, M. L.; Lowe, A. M.; Abbott, N. L. *J. Colloid Interface Sci.* **2006**, *304*, 459.
(16) Shah, R. R.; Abbott, N. L. *Langmuir* **2003**, *19*, 275.
(17) Shah, R. R.; Abbott, N. L. *Science* **2001**, *293*, 1296.
(18) Tingey, M. L.; Luk, Y. Y.; Abbott, N. L. *Adv. Mater.* **2002**, *14*, 1224.
(19) Boden, N.; Bushby, R. J.; Martin, P. S.; Evans, S. D.; Owens, R. W.; Smith, D. A. *Langmuir* **1999**, *15*, 3790.
(20) Evans, S. D.; Allinson, H.; Boden, N.; Henderson, J. R. *Faraday Discuss.* **1996**, 37.
(21) Alkhairalla, B.; Allinson, H.; Boden, N.; Evans, S. D.; Henderson, J. R. *Phys. Rev. E* **1999**, *59*, 3033.
(22) Alkhairalla, B.; Boden, N.; Cheadle, E.; Evans, S. D.; Henderson, J. R.; Fukushima, H.; Miyashita, S.; Schonherr, H.; Vancso, G. J.; Colorado, R.; Graupe, M.; Shmakova, O. E.; Lee, T. R. *Europhys. Lett.* **2002**, *59*, 410.
(23) Evans, S. D.; Allinson, H.; Boden, N.; Flynn, T. M.; Henderson, J. R. *J. Phys. Chem. B* **1997**, *101*, 2143.
(24) Cheng, Y. L.; Batchelder, D. N.; Evans, S. D.; Henderson, J. R. *J. Phys. Chem. B* **1998**, *102*, 5309.
(25) Cheng, Y. L.; Batchelder, D. N.; Evans, S. D.; Henderson, J. R.; Lydon, J. E.; Ogier, S. D. *Liq. Cryst.* **2000**, *27*, 1267.
(26) Bramble, J. P.; Evans, S. D.; Henderson, J. R.; Anquetil, C.; Cleaver, D. J.; Smith, N. J. *Liq. Cryst.* **2007**, *34*, 1059.
(27) Bramble, J. P.; Evans, S. D.; Henderson, J. R.; Atherton, T. J.; Smith, N. J. *Liq. Cryst.* **2007**, *34*, 1137.
(28) Jerome, B. *Rep. Prog. Phys.* **1991**, *54*, 391.
(29) Jerome, B. *Handbook of Liquid Crystals*; Wiley-VCH: Weinheim, 1998; Vol. II.
(30) Sridharamurthy, S. S.; Cadwell, K. D.; Abbott, N. L.; Jiang, H. *Smart Mater. Struct.* **2008**, *17*, 012001.
(31) Yang, K. L.; Cadwell, K.; Abbott, N. L. *Sens. Actuators, B* **2005**, *104*, 50.
(32) Yang, K. L.; Cadwell, K.; Abbott, N. L. *J. Phys. Chem. B* **2004**, *108*, 20180.
(33) Attard, G. S.; Bartlett, P. N.; Coleman, N. R. B.; Elliott, J. M.; Owen, J. R.; Wang, J. H. *Science* **1997**, *278*, 838.
(34) Brake, J. M.; Abbott, N. L. *Langmuir* **2007**, *23*, 8497.
(35) Dalmolen, L. G. P.; Egberts, E.; Dejeu, W. H. *J. Phys. (Paris)* **1984**, *45*, 129.
(36) Dalmolen, L. G. P.; Picken, S. J.; Dejong, A. F.; Dejeu, W. H. *J. Phys. (Paris)* **1985**, *46*, 1443.
(37) Chen, W. P.; Ritchie, G.; Burstein, E. *Phys. Rev. Lett.* **1976**, *37*, 993.
(38) Ushioda, S.; Sasaki, Y. *Phys. Rev. B* **1983**, *27*, 1401.
(39) Corn, R. M.; Philpott, M. R. *J. Chem. Phys.* **1984**, *80*, 5245.
(40) Kurosawa, K.; Pierce, R. M.; Ushioda, S.; Hemminger, J. C. *Phys. Rev. B* **1986**, *33*, 789.
(41) Nemetz, A.; Fischer, T.; Ulman, A.; Knoll, W. *J. Chem. Phys.* **1993**, *98*, 5912.
(42) Harrand, M.; Masson, M. *J. Chem. Phys.* **1987**, *87*, 5176.
(43) Yahiaoui, B.; Masson, M.; Harrand, M. *J. Chem. Phys.* **1990**, *93*, 6047.
(44) Bousquet, C.; Masson, M.; Harrand, M. *J. Raman Spectrosc.* **1995**, *26*, 273.
(45) Futamata, M. *Langmuir* **1995**, *11*, 3894.
(46) Futamata, M. *J. Phys. Chem.* **1995**, *99*, 11901.
(47) Futamata, M.; Borthen, P.; Thomassen, J.; Schumacher, D.; Otto, A. *Appl. Spectrosc.* **1994**, *48*, 252.
(48) Lin, X. F.; Ren, B.; Yang, Z. L.; Liu, G. K.; Tian, Z. Q. *J. Raman Spectrosc.* **2005**, *36*, 606.
(49) Fukushima, H.; Tamaki, T. *J. Phys. Chem. B* **2002**, *106*, 7142.
(50) Zhang, H. L.; Evans, S. D.; Critchley, K.; Fukushima, H.; Tamaki, T.; Fournier, F.; Zheng, W.; Carrez, S.; Dubost, H.; Bourguignon, B. *J. Chem. Phys.* **2005**, *122*, 224707.
(51) Han, M.; Hara, M. *J. Am. Chem. Soc.* **2005**, *127*, 10951.
(52) Kumar, S.; Pal, S. K. *Liq. Cryst.* **2005**, *32*, 659.
(53) Ganesh, V.; Pal, S. K.; Kumar, S.; Lakshminarayanan, V. *J. Colloid Interface Sci.* **2006**, *296*, 195.
(54) Ganesh, V.; Pal, S. K.; Kumar, S.; Lakshminarayanan, V. *Electrochim. Acta* **2007**, *52*, 2987.
(55) Agarwal, A.; Suresh, K.; Pal, S. K.; Kumar, S. *J. Chem. Phys.* **2007**, *126*, 164901.
(56) Rossi, F. *Rev. Sci. Instrum.* **1992**, *63*, 3744.
(57) Rossi, F. *Rev. Sci. Instrum.* **1992**, *63*, 4174.
(58) Taylor, D. M. *J. Electrost.* **2001**, *51*, 502.
(59) Novotny, V. J.; Karis, T. E. *Appl. Phys. Lett.* **1997**, *71*, 52.
(60) Cheadle, E. M. Characterisation of Self-Assembled Monolayers; Ph.D. Thesis, University of Leeds, 2002.
(61) Allara, D. L.; Nuzzo, R. G. *Langmuir* **1985**, *1*, 52.
(62) Evans, S. D.; Ulman, A. *Chem. Phys. Lett.* **1990**, *170*, 462.
(63) Taylor, D. M.; Bayes, G. F. *Phys. Rev. E* **1994**, *49*, 1439.
(64) Demchak, R. J.; Fort, T. *J. Colloid Interface Sci.* **1974**, *46*, 191.
(65) Only the normal components of the dipoles will contribute to the surface potential.
(66) Dunmur, D. A.; Manterfield, M. R.; Miller, W. H.; Dunleavy, J. K. *Mol. Cryst. Liq. Cryst.* **1978**, *45*, 127.
(67) Nakagawa, Y.; Sawada, K.; Masuda, Y. *Mol. Cryst. Liq. Cryst.* **1981**, *67*, 283.
(68) Gray, G. W.; Mosley, A. *Mol. Cryst. Liq. Cryst.* **1976**, *35*, 71.
(69) Huang, K.; Fuller, G. G. *Liq. Cryst.* **1998**, *25*, 745.
(70) Jen, S.; Clark, N. A.; Pershan, P. S.; Priestley, E. B. *J. Phys. Chem.* **1977**, *66*, 4635.
(71) Ten-second exposure times were used to acquire the spectra corresponding to each point, leading to acquisition times for complete SPR Raman intensity curves of 20−30 min, depending on the angular range scanned.
(72) *Raether Surface Plasmons on Smooth and Rough Surfaces*; Springer-Verlag: Berlin, 1988; Vol. 111.
(73) Knoll, W. *Annu. Rev. Phys. Chem.* **1998**, *49*, 569.
(74) Cheadle, E.; Batchelder, D. N.; Evans, S. D.; Zhang, H. L.; Fukushima, H.; Miyashita, S.; Graupe, M.; Puck, A.; Shmakova, O. E.; Colorado, R., Jr.; Lee, T. R. *Langmuir* **2001**, *17*, 6616.
(75) Graupe, M.; Koini, T.; Wang, V. Y.; Nassif, G. M.; Colorado, R.; Villazana, R. J.; Dong, H.; Mirura, Y. F.; Shmakova, O. E.; Lee, T. R. *J. Fluorine Chem.* **1999**, *93*, 107.
(76) Laibinis, P. E.; Whitesides, G. M. *J. Am. Chem. Soc.* **1992**, *114*, 1990.
(77) Chu, K. C.; Chen, C. K.; Shen, Y. R. *Mol. Cryst. Liq. Cryst.* **1980**, *59*, 97.
(78) Rothenhausler, B.; Knoll, W. *Surf. Sci.* **1987**, *191*, 585.
(79) Noble-Luginbuhl, A. R.; Nuzzo, R. G. *Langmuir* **2001**, *17*, 3937.

JP907497P